Flexible 3D Printed Acrylic Composites based on Polyaniline/Multiwalled Carbon Nanotubes for Piezoresistive Pressure Sensors

Goretti Arias-Ferreiro, Aurora Lasagabáster-Latorre, Ana Ares-Pernas, M. Sonia Dopico-García, N. Pereira, P. Costa, S. Lanceros-Mendez, and María-José Abad*

The development of tunable UV-curable polymeric composites for functional applications, taking into consideration environmental issues and additive manufacturing technologies, is a research topic with relevant challenges yet to be solved. Herein, acrylic composites filled with 0–3 wt.%. polyaniline/ multiwalled carbon nanotubes (PANI/MWCNT) are prepared by Digital Light Processing (DLP) in order to tailor morphology, thermal, mechanical, and electromechanical properties. Viscosity, real-time infrared spectroscopy, and cure depth tests allow optimizing resin composition for suitable DLP printing. 2 wt.% is the maximum filler content reproducibly embedded in the polymer matrix. The advantages of PANI/MWCNT (50/50 wt.%) compared with single-component composites include safety issues, enhanced printability, increased electrical conductivity and thermal stability, and lower electrical percolation threshold (0.83 wt.%). Above this threshold the composites display excellent piezoresistive response, no hysteresis, and stability for over 400 compression cycles. The pressure sensibility (PS) of 2 wt.% composites decreases with applied pressure from PS ≈ 15 to 0.8 Mpa^{-1} for maximum pressures of 0.02 and 0.57 MPa, respectively. A proof-of-concept of the functionality of the novel materials is developed in the form of a tactile sensor, demonstrating their potential for pressure sensing applications as cost-effective, sustainable, and flexible materials for printed electronics.

1. Introduction

In the last decade, society demands the development of smart and multifunctional materials in order to satisfy the current digitalization paradigm in the scope of industry 4.0 and Internet of Things (IoT).[1–3] In this context, increasing attention has been focused on flexible and wearable sensing devices due to the large array of possible applications such as smart interiors, human health monitoring, and wearable electronics,[4–6] among others. Specifically, pressure and strain sensors are among the most demanded types of sensors. Based on the transduction mechanism, three main types of sensors can be developed: piezoelectric, piezoresistive, and capacitive sensing mechanisms.[5,7–9] Piezoresistive sensors are among the most used ones, being usually composed of electrically conductive films coupled with flexible substrates. When composite structures are stretched, microstructural changes lead to the modification of the electrical resistance as a function of the applied strain. Further, they combine great

G. Arias-Ferreiro, A. Ares-Pernas, M. S. Dopico-García, M.-J. Abad
Universidade da Coruña
Campus Industrial de Ferrol
Grupo de Polímeros-CIT
Campus de Esteiro, Ferrol 15403, Spain
E-mail: maria.jose.abad@udc.es
A. Lasagabáster-Latorre
Dpto Química Orgánica I
Facultad de Óptica y Optometría
Universidad Complutense de Madrid
Arcos de Jalón 118, Madrid 28037, Spain

N. Pereira, P. Costa, S. Lanceros-Mendez
Physics Centre of Minho and Porto Universities (CF-UM-UP)
University of Minho
Braga 4710-057, Portugal
N. Pereira, P. Costa
Laboratory of Physics for Materials and Emergent Technologies
LapMET
Lisboa 02-097, Portugal
S. Lanceros-Mendez
BCMaterials
Basque Center for Materials
Applications and Nanostructures
UPV/EHU Science Park
Leioa 48940, Spain
S. Lanceros-Mendez
IKERBASQUE
Basque Foundation for Science
Bilbao 48009, Spain

**ADVANCED
SCIENCE NEWS**
www.advancedsciencenews.com

**ADVANCED
ELECTRONIC
MATERIALS**
www.advelectronicmat.de

sensitivity and fast frequency response with a simple sensor structure.[10]

The manufacture and materials used in the production of a given sensor are key factors in its performance and applicability. The use of 3D printing technologies in electronics has great potential since it allows the integration of sensors, conductors, and devices with different electronic functions in the manufacturing process of the 3D object,[11,12] and has boosted the development of diverse photocurable flexible materials.[13] Nowadays, stereolithography (SLA) and digital light processing (DLP) can be considered among the most important and novel Additive Manufacturing technologies. The methods are based on the layer-by-layer solidification of a liquid photosensitive resin via ultraviolet (UV)-light exposure.[14]

In general, polymer-based piezoresistive sensing films are composed of a polymer matrix and conductive fillers. Among the frequently used fillers, the following stand out: multi-walled carbon nanotubes (MWCNTs),[15] graphene,[16] and polyaniline (PANI).[5,8] Electrical, mechanical, thermal, and electromechanical properties are affected by the filler type, content, and aspect ratio.[7] Regarding the matrix, the typical ones are thermoplastics, elastomers, and hydrogels.[17] Research into new materials enables the implementation of new features as well as increases the range of applications but it also leads to significant challenges in the choice of structural design and material compatibility.

Among conductive fillers, PANIs are increasingly being used, due to their electrical response, environmental stability, simple synthesis, and low cost.[18] However, the amount of pure PANI that can be embedded in a photocurable resin is insufficient to obtain a high electrical conductivity,[9,19,20] in the range of semiconductor materials, needed to fabricate piezoresistive sensors. In this context, modifying the synthesis of PANI with the introduction of another conductive filler, such as MWCNTs, allows to increase the electrical properties of the composites, as well as the thermal stability with respect to neat PANI;[21–25] on the other hand, this strategy facilities the handling of MWCNT, avoiding the risk of inhaling the toxic dust aerosols which might be set free due to their tiny size and ultralight weight;[26] it further avoids aggregation and favor dispersion in the photocurable resin. Therefore, PANI/MWCNTs hybrid materials could be considered as an excellent candidate for the fabrication of sensor devices, energy conversion systems, and storage or supercapacitors due to their specific electrical properties.[5,8,27–29] Up to now, there are some studies dealing with the incorporation of PANIs[19,30–32] and MWCNTs,[33–36] separately, in light-curing matrix, but no reports have been found focusing on the addition of PANI/MWCNTs to UV curable resins.

The main target of this work is the design of novel acrylic conductive resins filled with PANI/MWCNT to be printed by DLP, suitable for the manufacture of piezoresistive sensors. First, 50/50 wt.% PANI/MWCNT composites were obtained through in situ polymerization of aniline in a suspension of MWCNT and fully characterized. Then, a complete printability study of the novel conducting composites was carried out, including an analysis of the microstructure and physicochemical properties of printed samples. The electromechanical response of the developed materials has been evaluated and a proof of concept touch device demonstrated, showing the potential of the 3D printed materials for sensing applications.
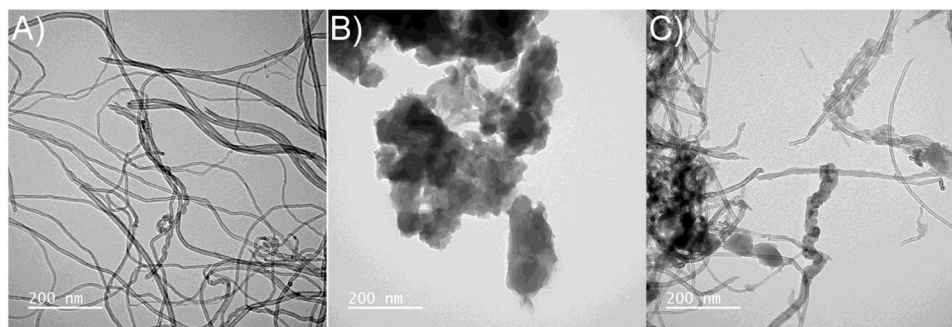
2. Results and Discussion

2.1. Characterization of PANI/MWCNT Filler

The morphological and structural differences between PANI/MWCNT and its constituents have been studied. TEM and SEM images were obtained to analyze the morphology of the MWCNTs, PANI/MWCNT, and PANI (**Figure 1** and Figure S1, Supporting Information).

The TEM image of MWCNTs (Figure 1A) shows a long fiber shape of about 11 nm of thickness. Similarly, SEM photographs confirmed a highly entangled network structure (Figure S1, Supporting Information), which is responsible for the difficulty in dispersing the MWCNTs in the polymer resin and the relatively low dispersion of the conductive filler in most solvents.[37]

Concerning PANI-HCl, individual PANI nanorods of about 130×35 nm are interwoven and stacked together in disordered and densely packed aggregates[9] (Figure 1B). When PANI is synthesized in the presence of MWCNTs to obtain PANI/MWCNT composite, a deposition of PANI on the MWCNTs surface occurs,[24] increasing the fibers' thickness to 21 nm (Figure 1C). The coated MWCNTs (Figure 1C) show a well discernible internal cavity, confirming that PANI interacts exclusively at the outer surface of the MWCNT. This is an expected result since the polymerization of aniline inside the CNT is hindered by the restricted access of reactants to the interior of the CNT.[21] Similar behavior of the PANI deposition has been reported in the literature in the presence of MWCNTs, varying

Figure 1. TEM images of A) MWCNT, B) PANI, and C) PANI/MWCNT.

**ADVANCED
SCIENCE NEWS**

www.advancedsciencenews.com

**ADVANCED
ELECTRONIC
MATERIALS**

www.advelectronicmat.de

the PANI coating as a function of the ratio of aniline/MWCNT in the reaction medium.[38] PANI/MWCNT tends to present a fiber smooth surface with a size from 20 to 28 nm.[24]

The elemental analysis of MWCNT revealed the presence of a high atomic concentration of oxygen 13%.wt.[39] Further, the elemental analysis of PANI/MWCNT leads to 5.28 wt.% N; 66.74% C; 2.55% H; 1.51% S. The C/N atomic ratio derived from these data, 12.64, is nearly twice the value of the ratio of pristine PANI, 5.97.[40] The experimental wt.% of PANI in the PANI/MWCNT composite was determined, taking as reference the elemental composition of the pure PANI, according to Equation (1). The calculated experimental PANI content is 49.7 ± 0.7 wt.%, whereas the expected theoretical content was 54.5% considering the yield of the reaction; hence, the composite is a mixture of 50:50 PANI:MWCNT.

The X-ray powder diffraction scans display the typical powder diffraction patterns for MWCNTs[41] and semicrystalline PANI emeraldine salt[42] (Figure S2A, Supporting Information). In the diffractogram of the PANI/MWCNT composite, the peaks of both components are superposed, although the strong peak at $2\theta = 26°$, related with the average interlayer spacing within each nanotube, dominates the spectrum. Due to peak overlapping, it is difficult to confirm that any additional order in the molecular arrangement in either PANI or MWCNT has been introduced as a result of the interaction of both components,[22,23,43] nor the opposite situation.[22]

Concerning the Raman spectrum, the profile of PANI/MWCNT is similar to the spectrum of MWCNT with some contributions of PANI absorption in the region between 1700 and 1100 cm^{-1} (Figure S2B, Supporting Information). The intensity ratio I_D/I_G for the D-band and G-band is widely used for characterizing the defect quantity in graphitic materials. The I_D/I_G ratio of pristine MWCNT, 1.30, is indicative of a highly defective functionalized outer surface.[44] In relation to PANI/MWCNT, as the PANI bands overlap with the nanotubes G and D bands, caution must be taken on assessing the I_D/I_G values decrease to 1.15. Nonetheless, there is also a neat decrease in the D´ band intensity, which may imply that PANI on the MWCNT surface improves the graphite degree of PANI/MWCNT composites.[45]

Opposite to the Raman and XRD analysis, distinct shifts and intensity changes of PANI bands are clearly discernible in the FTIR spectrum of PANI/MWCNT, revealing that the electronic behavior differed from the one of pristine PANI (Figure S3, Supporting Information). The modifications, discussed in detail in the Supporting Information, point to conformational changes of PANI, from a coil-like structure to an extended one, as a result of strong π-π conjugated interactions between the quinoid rings and carbon nanotubes, and enhancement of all the bands related with electron delocalization, suggesting that carbon nanotubes may function as a chemical dopant for PANI conductivity, thus enhancing the conductivity of the polymer chains.[25] Further, the FTIR spectrum confirms the functionalization of the MWCNT with carboxyl and OH groups, predicted by elemental analysis,[39] allowing additional H- bond interactions with the N-H groups of PANI. Briefly, as suggested by Wu and Lin[46] π-π interactions together with hydrogen bonding take place between the amino groups of PANI and the carboxylic groups of functionalized MWCNT, rather than electrostatic interactions.

Figure S4, Supporting Information, shows the UV–vis spectra of PANI and PANI/MWCNT. Both PANIs exhibit two bands at 470 and >800 nm in the visible region, due to π-polaron and polaron-π* bands transitions, corroborating that PANI deposited on the MWCNT surface is in the form of emeraldine salt.[9] Nevertheless, the presence of MWCNTs in the PANI/MWCNT composite increase the absorptivity at 405 nm (DLP wavelength) with respect to pure PANI from approximately 5.2 to 8.4 l. g^{-1} cm^{-1} (see Section S1.1, Supporting Information). Hence, the maximum amount of PANI/MWCNT that can be incorporated into the acrylic resin during the printing process is expected to decrease with respect to previous studies with PANI,[9,40,47] due to its higher blocking effect of UV light retarding the polymerization.[48]

The thermal properties of PANI and PANI/MWCNT are described in Section S1.3 and Table S1, Supporting Information. As the MWCNT are stable over the whole investigated temperature range, the thermal stability of PANI/MWCNT is greatly increased with respect to pure PANI[49] (Figure 4A). The additional weight loss detected at 786 °C in the DTG thermogram of PANI/MWCNT, has been ascribed to the decomposition of a thin layer of PANI deposited directly on the surface of the MWCNTs[50] and more than 70 wt.% of PANI/MWCNT mass remains as a residue, in contrast with the 44 wt.% of pristine PANI. Thus, better thermal stability supports the strong bonds between PANI and MWCNT described by FTIR.[25,38]

2.2. Characterization of Acrylic 3D Printed Composites

2.2.1. Prepolymerization Studies

Viscosity is a key parameter in a photocurable 3D printable resin to ensure the adhesion of the photoresin to the printing platform and the subsequent adhesion between layers.[33,47] To begin with, the effect of PANI/MWCNT filler on the steady shear viscosity of the liquid resin as a function of shear rate viscosity was studied at room temperature (Figure S5, Supporting Information). In addition, the viscosity values at 1 s^{-1} for all tested formulations are summarized in **Table 1**.

The viscosity of the loaded polymer increased from 0.011 to 0.103 Pa s at 1 s^{-1} as the conductive loadings augmented from 0 to 3 wt.%. The rise in viscosity with increasing filler concentration is due to the higher interactions between the dispersed PANI/MWCNT, which inhibit the normal flow of polymeric chains.[33] The viscosity values achieved for 2 and 3 wt.% PANI/MWCNT are comparable to the viscosity obtained in previous studies for 3.5 wt.% PANI-HCl suspended in the same acrylic formulation (0.078 Pa s at 1 s^{-1}). Under the circumstances, PANI/MWCNT conductive filler slightly raises the viscosity of the photoresin and limits the quantity that can be added to the formulation to 2 wt.%, to achieve good printability and electrical conductivity. This level is well below reported values which used PANI (up to 6 wt.%)[19,20,40,47] or graphene (5 wt.%),[51] but it is enough to obtain successful properties. However, regarding previous studies using only MWCNTs, the amount of filler introduced in 3D photopolymerizable resins was only 0.5 wt.% since it

2200590 (3 of 13)

Table 1. Samples formulation, 3D printer exposure times, viscosity at 1 s^{-1}, induction period, maximum rate of polymerization (R_P) and ultimate degree of double bond conversion (%DBC) at 9 mW cm^{-2} obtained from kinetic of polymerization.

Sample	Filler [wt.%]	Exposure time [s]	Bottom exposure [s]	Viscosity [Pa s] 1 s^{-1}	Induction period [s]	Max. rate of polymerization (R_P) [mol L^{-1} s^{-1}]	Ultimate DBC [%]
T7PC0	0	1	15	0.011	<8	62.0 ± 0.6	98.0 ± 0.2
T7PC05	0.5	2	20	0.033	<13	24.4 ± 0.4	98.6 ± 0.7
T7PC1	1	2	20	0.036	<13	8.7 ± 1.5	97.9 ± 0.8
T7PC125	1.25	4	30	–	–	–	–
T7PC15	1.5	5	30	0.074	67 ± 3	4.1 ± 0.1	95.0 ± 0.7
T7PC175	1.75	15	45	–	–	–	–
T7PC2	2	15	60	0.110	73 ± 2	3.8 ± 1.1	93.1 ± 1.6
T7PC3	3	40	100	0.103	–	–	–

was limited by their viscosity values of 12[52] and 37 Pa s[33] at 1 s^{-1}. Commercial formulations (zABS and zDENTAL from UNIZ TECHNOLOGY LLC) showed viscosity values at 1 s^{-1} of 0.4 and 0.8 Pa s,[40] respectively; therefore, the corresponding values of the in-house formulated resins are in the same order of magnitude.

The effect of the amount of PANI on the photocuring rate of the acrylate copolymer has been investigated by in situ ATR-FTIR spectroscopy. The experiments were carried out on dispersions of acrylic resin with 0, 0.5, 1, 1.5, and 2 wt.%. PANI/MWCNT exposed to UV light. The degree of double bond conversion (%DBC), calculated with Equation (2), was plotted versus irradiation time (**Figure 2**). The maximum rate of polymerization(R_P), determined with Equation (3), together with the induction period and ultimate degree of double bond conversion, are compiled in Table 1.

Minor variations in the induction period and no changes in the ultimate degree of conversion are observed for PANI/MWCNT contents ≤1 wt.%. Nevertheless, longer retardation in polymerization initiation and slightly lower final conversions

are seen for higher filler contents. By contrast, there is a pronounced exponential decrease in the rate of photopolymerization as shown in Figure 2 inset (r^2 = 0.995) upon increasing the PANI/MWCNT content from 0.5 wt.% onwards. This is a very well-known phenomenon mainly due to the strong absorption of UV light by both the MWCNTs filler[33] and PANI, which strongly compete with the light adsorption of the photoinitiator.[48] The long induction period observed for PANI/MWCNT composites could also be due to the reported role of PANI as a free radical scavenger.[53]
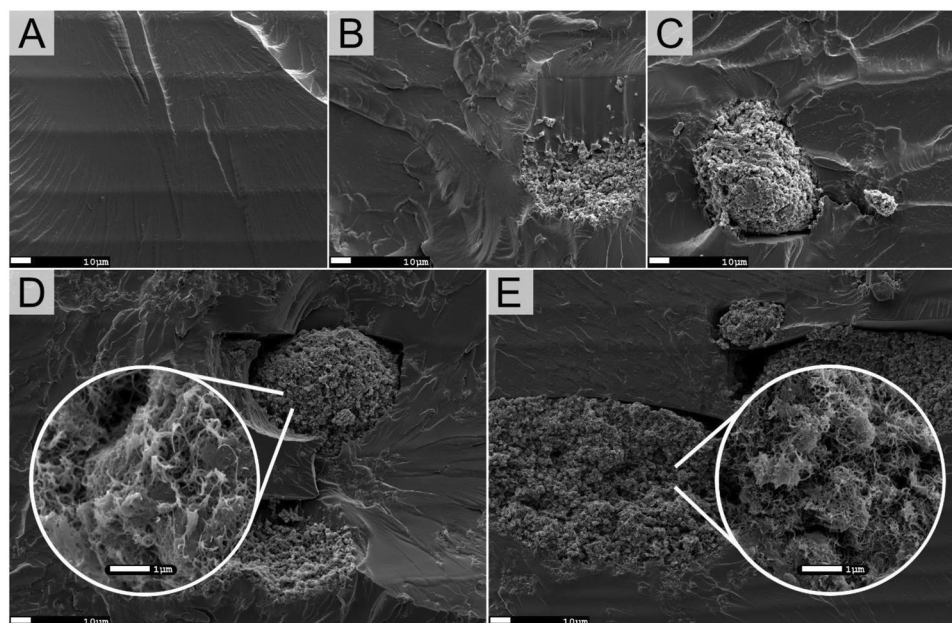
2.2.2. Morphological Properties of the 3D Printed Samples

The morphological differences between the 3D printed samples of pure acrylate resin and the PANI/MWCNT composites were evaluated by SEM (**Figure 3**).

Horizontal lines corresponding to the individual layers formed during the 3D printing process can be observed in the cryo-fractured cross-section of the pure acrylate film (Figure 3A). Upon increasing filler loading, the individual layers can still be perceived together with an increase in the features of crack-propagation and porosity. At filler contents lower than 1 wt.%, small and dispersed filler clusters, well embedded in the polymer matrix, can be observed (Figure 3B); but above this content, together with this segregated and well-dispersed network, larger filler aggregates randomly appear protruding from cracks and pores (Figure 3C–E), revealing segregation from the polymer matrix. This increase in the aggregates' size with filler content is due to the strong aggregation between PANI/MWCNT or its individual components related to π-π interactions, hydrogen bonding, dipole–dipole, and London forces between the PANI chains and MWCNT, whereas the lack of interaction between the matrix and the filler has been confirmed by Raman and FTIR spectroscopy (results not shown). These images are consistent with the sharp increase in printing time to achieve adhesion to the platform and the increase in the viscosity values observed in the resin formulations upon 1% (Table 1, Figure S5, Supporting Information). Briefly, this result reveals that the interlayer porosity of the samples may cause weak interfaces and can affect the viability of the 3D print, as well as the overall strength of the printed object.[9,47,54]
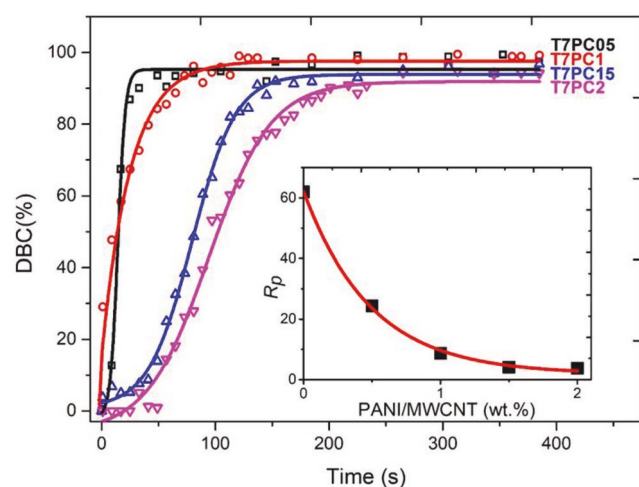
Figure 2. Conversion curves versus irradiation time for acrylic dispersions with 0.5, 1, 1.5, and 2 wt.% PANI/MWCNTs. The experimental data (symbols) were fitted with Boltzmann sigmoidal equation (lines). (For clarity purposes the conversion curve for neat acrylic resin is not shown because it overlaps that of T7PC05).

ADVANCED
Science News
www.advancedsciencenews.com

ADVANCED
ELECTRONIC
MATERIALS
www.advelectronicmat.de

Figure 3. Representative SEM images of A) pure acrylic resin, B) T7PC05, C) T7PC1, D) T7PC15, and E) T7PC2 with magnitude amplification of 500× for the main image and 10 000× for the insets.

### 2.2.3. Thermal, Mechanical, and Electrical Properties of 3D Printed Samples

The thermal behavior of the acrylate composites was evaluated by TGA. The results are displayed in **Figure 4**A and Table S1, Supporting Information, and detailed in the Supporting Information. In accordance with previous papers dealing with a similar polymer matrix, the pure acrylic resin can be considered thermally stable up to 375 °C (T_{10}) and leaves a very small residue of 2.9 wt.% at 700 °C.[40] Likewise, acrylic composites display very similar degradation profiles with respect to neat polymer with the exception of TPC3, which shows an additional weight loss of 14.5 wt.% ascribed to the evaporation of volatiles and PANI dopants, HCl o H_2SO_4. These are expected results due to the addition of fillers that absorb UV light, which at higher contents hinder the photopolymerization reaction.[9,40,48,35] From another point of view, some composites show an additional step at temperatures ≥700 °C in the DTG thermograms (not shown), assigned to the decomposition of a thin layer of PANI deposited directly on the surface of the MWCNTs[50] and the ash residues increase upon raising the content of Pani/MWCNT.

To evaluate the practical application of the 3D printed composites, mechanical uniaxial tensile tests till rupture were performed according to ISO 527 with at least five dog-bone-shaped specimens. From the stress–strain curves, depicted in Figure 4B, the modulus, stress at break, and elongation at break of the printed composites were calculated and presented in Table S2, Supporting Information.

No significant differences are observed in the Young modulus of PANI/MWCNT composites compared to pristine acrylic resin, within experimental error. By contrast, both the tensile strength and the elongation at break decreased around 50% for 1.5 and 2 wt.% PANI/MWCNT, reducing ductility. At any

rate, although a more brittle behavior is produced the samples retained flexibility. Similar results were obtained in a previous paper for PANI-HCl composites using the same acrylic matrix. These results are attributed to the cracks and pores observed by SEM, mainly located at the interface between layers, as is often observed in tray polymerization, especially in heterogeneous compounds with poor filler dispersion and lack of interaction between the matrix and the filler[47,54] In line with these explanations, Joo and Cho[20] did not observe significant variations in the stress-strain curves between DLP-3D printed samples of the pristine polyurethane matrix (PU) and the PU/PANI composites, in contrast to the reinforcing effects obtained with PU-graphene sheet composites. They suggested that the formation of PANI clusters retards the reinforcing effects on the ultimate strength of the PANI composites.[20] Furthermore, the addition of MWCNT contents between 0.3 and 0.6 wt.% to acrylic or polyurethane acrylated resins lead to a 50% reduction in Young modulus,[55] which was explained by the decrease of crosslinking density due to the negative influence of the filler in the photopolymerization reaction[33] and agglomeration or MWCNT clusters act as defects with respect to the mechanical response.[35]

Regarding the electrical properties, the PANI/MWCNT filler has an average electrical conductivity of 15.0 ± 1.8 S cm^{-1}, which duplicates the value of pristine PANI[47] and is in the range of good semiconductors and analogous to PANI/MWCNT composites synthesized by a similar procedure.[21] The electrical conductivity value of the pure acrylic resin is lower than 1.0×10^{-8} S cm^{-1}, which is the limit of detection of the measurement equipment. This value increases as the PANI/MWCNT content increases in the composites, as depicted in Figure 4C. The electrical percolation threshold of the PANI/MWCNT acrylic resin is graphically observed in the range of 0.5–2 wt.% PANI/MWCNT content, with an electrical conductivity
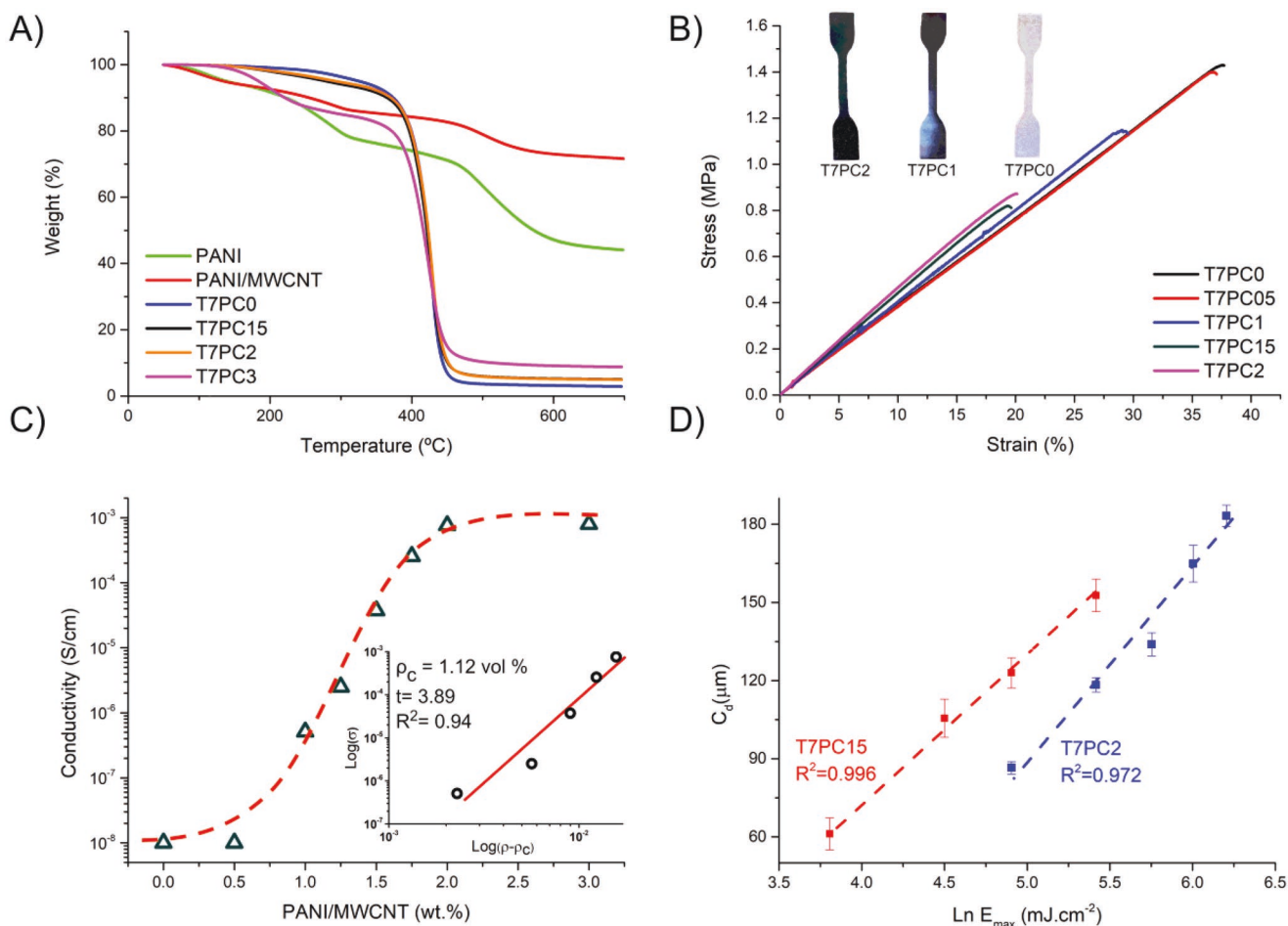
Figure 4. A) TGA curves of PANI, PANI/MWCNT, and the acrylic composites T7P0, T7PC15, T7P2, and T7PC3. B) Stress-strain behavior of acrylic composites (representative curves). C) Electrical conductivity of acrylic composites as a function of PANI/MWCNT content (curve for guiding the eyes). Inset: log–log plot of electrical conductivity versus $\rho\text{-}\rho_c$, and D) working curves of T7PC15 and T7PC2 composites exposed to 405 nm light (9 mW cm^{-2}).

increment from the detection limit of the equipment $(1.00 \pm 0.01) \times 10^{-8}$ to $(7.6 \pm 0.3) \times 10^{-4}$ S cm^{-1}, respectively. Further, within experimental error, the electrical conductivity tended to a plateau above 2 wt.% (reaching the maximum values) in accordance with the rheological results. Hence, these values are in the range of semiconductors and suggest the existence of a continuous network of PANI across the film. The data are slightly higher than those obtained in photocurable acrylic resins for DLP 3D printing employing only carbon nanotubes[33–35] or PANI[19,20,47] as conductive fillers. Until now, there are no data on electrical conductivity in DLP 3D printed composites using PANI/MWCNT filler.

The critical concentration of the conductive photoresin was mathematically determined using the percolation theory, where the electrical conductivity is given by the percolation threshold (ρ_c) following Equation (4) (Section 4.2.2). Therefore, the critical exponent related to the dimensionality of the system (t) can be determined from the slope of the log (σ) versus ($\rho\text{-}\rho_c$) representation.[56] From the data fit, shown in the inset of Figure 4C, the measured percolation threshold was close to $\rho_c = 1.12$ vol% (0.83 wt.%) and t is around 3.89. The percolation threshold is lower than the value calculated for neat PANI in the same polymer matrix in a previous work ($\rho_c = 2.9 \pm 0.6$ vol%).[40] Further, typically, $t \approx 1.6$–2.0 and $t \approx 1.1$–1.3 are found for 3D and 2D conductive networks, respectively. The t value of PANI/MWCNT is actually higher than the theoretical prediction, which might arise from the specific structure and properties.[58] Specifically, values of t above 3.75 suggest the existence of a strongly interconnected network, directly assembled between the fillers.[58]

The conductivity values achieved are higher than those reported for printable photocurable resins using other fillers such as nanoparticles of Ag (10^{-6}–10^{-11} S cm^{-1})[59,60] or reduced graphene oxide (rGO) (10^{-7} S cm^{-1}).[61] By contrast, some authors have reported higher conductivity[62] values in the order of 10^{-2}–10^{-3} S cm^{-1}, although using a much higher amount of fillers such as 6% of rGO[63] or 20% of PEDOT.[55] The use of high amounts of filler is not desirable considering their cost and the negative effect on the performance of the material.[63]

2.3. Printable Composites for Force Sensor Devices

Taking into account the electrical results, PANI/MWCNTs/acrylic composites above the electrical threshold could be

**ADVANCED
SCIENCE NEWS**

www.advancedsciencenews.com

**ADVANCED
ELECTRONIC
MATERIALS**

www.advelectronicmat.de

considered excellent candidates for electromechanical sensors under pressure stimulus.[65] To prove this assertion, the cure depth and the electromechanical properties of T7PC15 and T7PC2 were evaluated. Besides, a proof-of-concept was developed using a 3D printed sample with an appropriated electronic system to detect finger touch in a matrix of 5 × 5 sensors.

2.3.1. Jacobs Working Curves

This section characterizes the feasibility of the developed formulations for 3D DLP printing technology. Jacobs working curves, corresponding to T7PC15 and T7PC2, were created (Figure 4D). The correlation coefficients (R^2) of the logarithmic regression lines were 0.996 and 0.972, respectively. As previously stated, the light intensity of the 3D printer was 9 mW cm^{-2} and layer thickness (z) was set at 25 μm for all compositions. The exposure time for each formulation was set based on some preliminary tests and is shown in Table 1.

Based on Equation (5) (Section 4.2.3), the E_c, D_p, and C_d parameters were calculated. E_c is the starting point for the transition from liquid to solid (mJ cm^{-2}), D_p is the penetration depth (μm) of the light source into the resin and C_d is the cured depth (μm). Regarding T7PC15, the E_c, D_p, and C_d parameters were 15 mJ cm^{-2}, 56 μm, and 68 μm for a light irradiation dosage, E_o, of 45mJ cm^{-2}. In the case of T7PC2, the E_c, D_p, and C_d parameters were 44 mJ cm^{-2}, 73 μm, and 82 μm, calculated for a layer exposure of 135 mJ cm^{-2}. E_o values correspond to the products of the light intensity of the printer 9 mW cm^{-2} and an exposure time per layer of 5 and 15 s for T7PC1 and T7PC2, respectively.

As expected, increasing the amount of PANI/MWCNTs, greatly augmented the critical exposure (E_c) to induce polymerization with an increase of threefold E_c with only 0.5% more filler. These results are explained by its high UV absorption as previously shown by UV spectrometry. The same effect has been described for the addition of lignin,[65] carbon nanotubes,[33] and neat PANI.[40,47,48] Moreover, the value of E_c obtained for T7PC2 (45 mJ cm^{-2}) is higher than the values reported for commercial non-conductive resins by Bennet et al.[66] (<13 mJ cm^{-2}), which is explained by the presence of a large amount of filler. However, the E_c value (15 mJ cm^{-2}) for the T7PC15 sample is similar to commercial non-conductive resin values, which proves that this formulation, with semiconducting properties, could be easily used for the elaboration of complex 3D printed structures. Compared to previous formulations developed with 3.5% PANI-HCl[47] in a similar acrylate resin (E_c = 45 mJ cm^{-2}; 10^{-5} S cm^{-1} conductivity), the use of PANI/MWCNTs facilitates printability by diminishing or maintaining E_c while improving the level of conductivity (10^{-4} S cm^{-1}).

The D_p values (56 and 73 μm for TPC15 and T7PC2, respectively) lie within the low range of commercial resins without conductive fillers tested by Bennet et al. (53–568 μm).[66] Low D_p values have the advantage to allow accurate control of the polymerization process and minimal over-cure, although the disadvantage of higher building times.[67]

In DLP 3D printing, to obtain good adhesion between layers it is necessary that $C_d > z$, since the stiffness of a polymer below the gel point is not enough to endure the printing process.[47,68] Following this criterion, both formulations, T7PC15 and T7PC2 (C_d = 68–73 μm; z = 25 μm), are good candidates for satisfactory 3D printability of semiconductive objects.

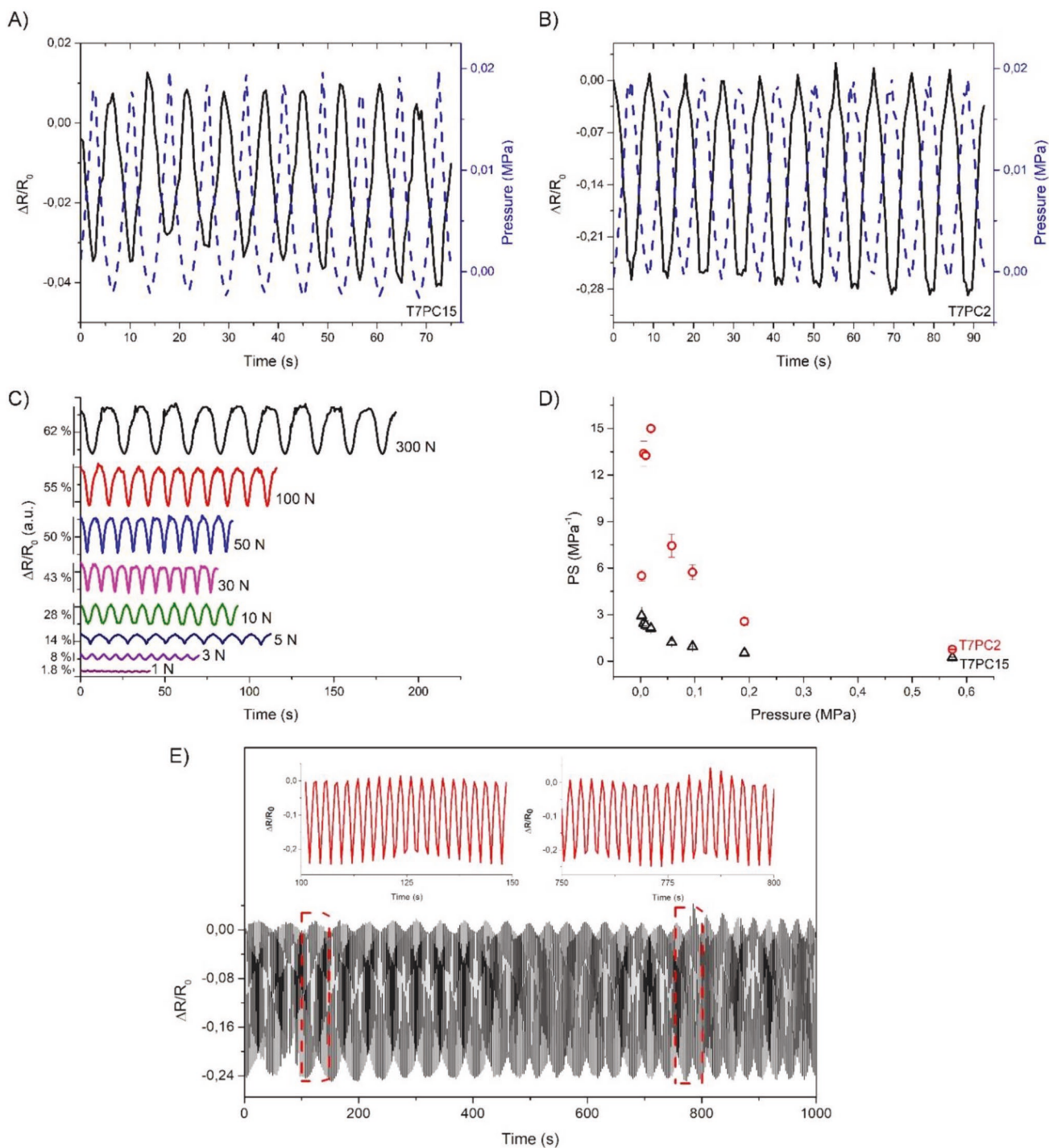### 2.3.2. Electromechanical Properties

Electromechanical compression tests (**Figure 5**) were performed for T7PC15 and T7PC2 in order to evaluate their sensitivity and linearity. The electromechanical response was calculated under 10 compressive loading-unloading cycles at a high range of loads between 1 to 300 N (equivalent to the pressure range from 2 kPa to 0.57 MPa).

Figure 5A,B shows the relative variation of resistance during 10 loading-unloading cycles for pressure changes up to 0.02 MPa at a strain rate of 1 and 5 mm min^{-1} for PANI/MWCNT composites with 1.5 and 2 wt.%, respectively. Electromechanical tests show the linearity between electrical resistance variation and applied pressure for both amounts of filler with a small hysteresis effect. Similar electromechanical linearity and cycling performance have been reported in composites with PANI[5,8] and MWCNTs.[7,64]

The experimental loading-unloading cycles as a function of applied force for T7PC2 formulations (similar performance for T7PC15) have been depicted in Figure 5C. The electromechanical performance for both composites as a function of the applied pressure is shown in Figure 5D, showing the pressure sensibility, PS, for several forces. Both composites present good linearity during the compression cycles and PS exponentially decreases with increasing applied pressure. T7PC15 composite, which lies just above the electrical threshold, shows a piezoresistive response near 3 MPa^{-1} for low pressures, which gradually decreases with applied pressure, owing to variations of filler-filler distance caused by compression of the filler network leading to its permanent deformation. This behavior has also been observed in CNT-based composites under compression electromechanical tests.[7,64] On the other hand, the T7PC2 composite, which has a higher electrical conductivity than T7PC15, also displays higher piezoresistive sensitivity throughout the tested pressure range; notwithstanding, the differences between both compositions are greater for the low-pressure range. T7PC2 achieves the maximum value of PS, 15 MPa^{-1}, when the applied force is 10 N, being 5 times higher than the PS value of T7PC15.

As expected, these values are lower than the sensitivities of previously reported sensors based on porous materials coated with PANI[5,69,70] or multilayer fibrous structures coated with PANI-nanospines;[8] notwithstanding, they are comparable to bulk piezoresistive pressure sensors filled with CNT.[7,64,71] These results demonstrate that additive manufacturing processes can be employed to design 3D printed materials for sensor applications. Even though the sensitivity is lower compared to foams, the sensitivity and linearity are compatible with a wide range of applications.

Further, the cycling stability of the T7PC2 sample is demonstrated by the small relative resistance changes for 400 loading-unloading cycles at 0.02 MPa of pressure, proving excellent durability and reliability (Figure 5E). The minimum

**ADVANCED
SCIENCE NEWS**

www.advancedsciencenews.com

**ADVANCED
ELECTRONIC
MATERIALS**

www.advelectronicmat.de

Figure 5. Electromechanical response of A) pressure and relative resistance variation as a function of time (up to 10 N or 0.02 MPa) for T7PC15 and B) T7PC2 composites. C) Time-dependent resistance changes of T7PC2 under different repetitive forces (1 to 300 N). D) Pressure sensibility up to 300 N (≈0.6 MPa) for T7PC15 and T7PC2 composites. E) Stability of T7PC2, potential piezoresistive pressure sensor, during 400 loading–unloading cycles at a force variation up to 10 N (0.02 MPa). Insets display the enlarged relative resistance changes, over 20 cycles, within 100–150 and 750–80 s, respectively.

and maximum electrical resistance remains similar throughout the cycles; hence, it is concluded that the mechanical stability of these composites is excellent and, therefore, they can be used as potential sensor materials.

2.3.3. Proof-of-Concept: Touch Sensing Device

The 3D printed composites based on the T7PC2 sample were used to fabricate a resistive matrix with 5 × 5 sensors for force

2200590 (8 of 13)
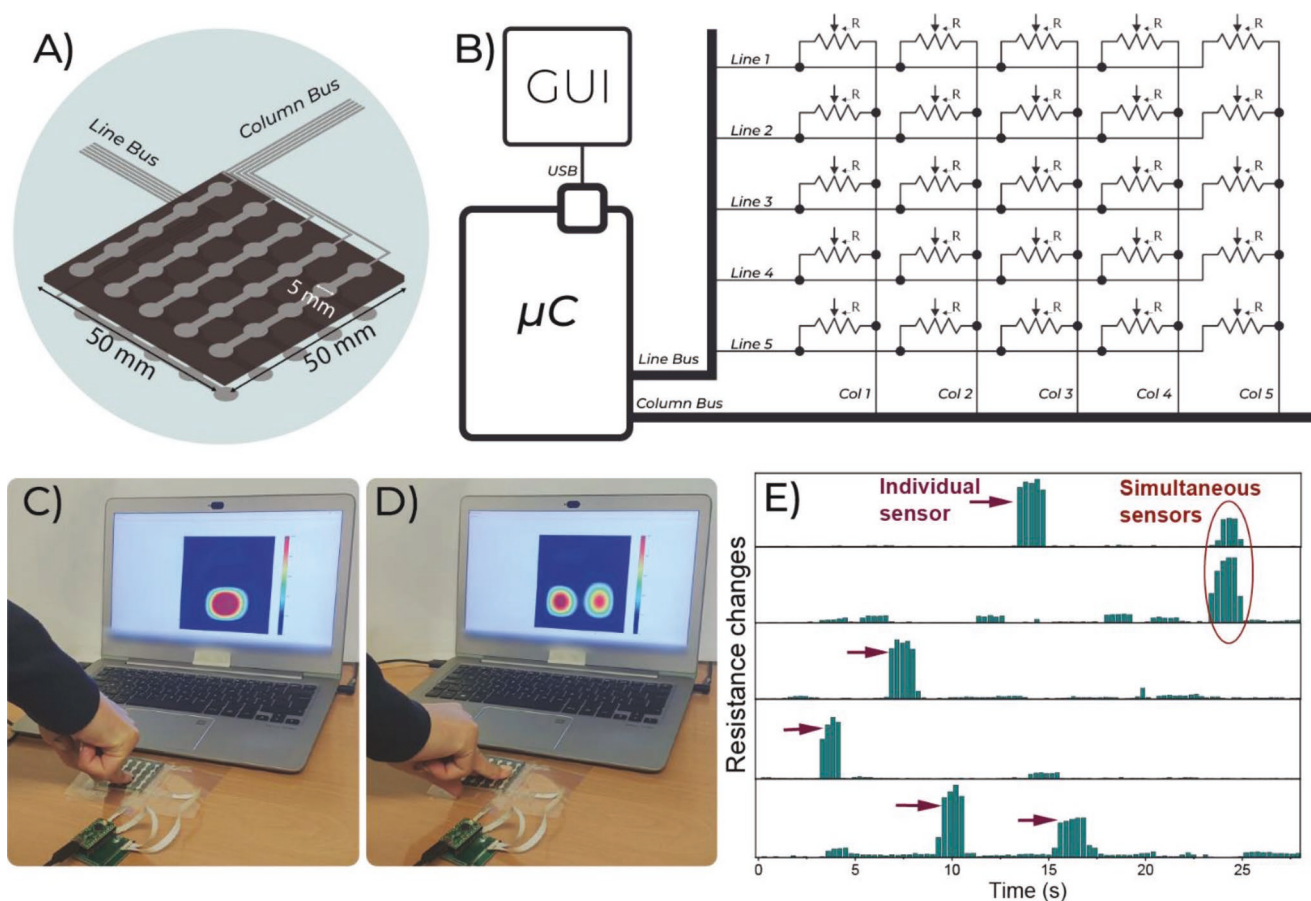
Figure 6. Diagram of the A) fabrication process with a 50 × 50 mm square pattern and B) electronic schematic of the connection of the resistive matrix with the microcontroller. Force detection with C) one finger and D) two fingers, with respective sensitivities of the system to the finger touch (E).

sensing. Commercial conductive silver nanoparticle ink (Metalon HPS-021LV from Novacentrix) was screen-printed on two commercial PET sheets with 100 µm of thickness from Dupont Teijin company (**Figure 6**A). The square pattern with dimensions of 50 × 50 mm (with circles of 5 mm), was screen printed to create an interdigitate system in volume, placing the sample between the conductive interdigitates. The developed 3D printed resistive film based on T7PC2 was placed and glued between the two PET sheets, controlling the air gap between the electrodes and the resistive film. The force sensors were connected to a microcontroller, Teensy -LC from PJRC, where the electrodes were connected to an internal voltage divider composed of the internal pull-up resistors in the analog-to-digital (ADC) pins. The firmware reads the resistance value between the column and the line of the matrix with the 12-bit ADC for all the 25 sensors (Figure 6B). The data is gathered and sent via serial port to a laptop. A graphic user interface (GUI) was developed to display and acquire the variation in resistance when a tactile force is applied. Figure 6C,D shows the variation in resistance when touching with one finger or two-finger simultaneously. In the chart, the variation of the color gradient from blue to red dictates the percentage of force that is being applied (low to high force, respectively).

In short, the proof-of-concept perfectly works when force is applied, and the signal can be observed and processed by the electronic system (Figure 6E), as can be appreciated in a Supporting Information video. Using this system, the printed composites can be used as sensors for detecting the tactile force exerted over the material.

3. Conclusion

Conductive acrylic composite resins filled with up to 3 wt.% PANI/MWCNTs have been prepared and printed by DLP to assess the influence of the filler content on the microstructure and physicochemical properties and, hence, their performance for pressure sensor applications. The viscosities of PANI/MWCNT filled acrylic composites are in the range of commercial resins, enabling adequate 3D printed settings in terms of D_p and E_c values. A maximum amount of PANI/MWCNTs around 2 wt.% can be successfully and reproducibly embedded in the photocurable resin, with important benefits in relation to single component composites. Compared with neat PANI, the use of PANI/MWCNTs facilitates DLP printing of conductive acrylate resins with lower filler content, as it increases their electrical conductivities by several orders of magnitude and lowers the electrical percolation threshold from 2.90 to 1.12 vol % (0.83 wt.%). Most importantly, from the point of view of environmental friendliness and occupational health, it avoids the

toxicity of handling the inhalable dust raised during the handling of MWCNTs. Further, although the ductility of the PANI/MWCNT composites is reduced with respect to the pristine polymer, they still maintain suitable flexibility for compression sensor devices.

The piezoresistive response demonstrates good reproducibility during cyclic loading without hysteresis with high piezoresistive sensitivities of ≈2–3 and ≈13–15 MPa^{-1} at pressure values between 1 and 10 N (0.002–0.02 MPa) for PANI/MWCNT filler contents of 1.5 and 2 wt.%, respectively. Further, the sensitivity of the latter is still as high as ≈7–3 MPa^{-1} in the medium pressure range (10 to 100 N or 0.02–0.2 MPa) with excellent repeatability over compression cycling solicitation, which proves that this formulation is suitable for sensing applications. Overall, the results confirm that composites based on PANI/MWCNT exhibit excellent piezoresistive responses, demonstrated by the implementation and testing of a force sensor, capable of detecting single and multiple tactile events in real-time.

4. Experimental Section

Materials and Samples Preparation: Aniline (ANI, 99.5%) and ammonium persulfate (APS, 99%) were obtained from Sigma-Aldrich (St. Louis, MO, USA) and Acros (Geel, Belgium) respectively. Hydrochloric acid (HCl, 37%) and methanol (MeOH) were purchased from Scharlau (Sentmenat, Spain). MWCNT was provided by Nanocyl (reference NC7000, purity of 90%, 1.5 mm length, and an outer mean diameter of 9.5 nm). Water was purified with an Elix 3 system (Millipore, Molsheim, France). Ethylene glycol phenyl ether acrylate (EGPEA, molecular weight = 192.21 g mol^{-1}); crosslinker 1,6-hexanediol diacrylate (HDODA, molecular weight = 226.27 g mol^{-1}), and the photoinitiator, diphenyl (2,4,6- trimethylbenzoyl) phosphine oxide (TPO, molecular weight = 348.37 g mol^{-1}) were purchased from Sigma-Aldrich (St. Louis, MO, USA). 2-Propanol obtained from Scharlau (Sentmenat, Spain) was employed to clean the samples after 3D printing.

Preparation of PANI/MWCNT Filler: MWCNT were coated with PANI in situ adapting the method described by Konyushenko et al.[21] and Stejskal et al.[72] for the oxidative polymerization of aniline. Aniline hydrochloride (5 g) was dissolved in 100 mL ethanol. 4 g of MWCNT were added to the monomer solution in the reactor and stirred for 60 min. The oxidant ammonium peroxydisulfate (APS, 11,4 g) was dissolved in 100 mL water and added dropwise to the monomer/MWCNT mixture to initiate the reaction. The polymerization reaction was carried out under mechanic stirring (150 rpm) with a refrigeration system (<6 °C) for 24 h. The resulting product was filtered under vacuum and washed with three 100 mL portions of 0.2 м HCl and 100 mL of acetone. PANI/MWCNT was obtained as a very dark green powder after drying for 24 h at 60 °C in a vacuum oven. The yield recovered was 8.8 g. For comparison, neat PANI has been prepared as above but in the absence of MWCNT.

Preparation and Printing of Acrylic Composites: Samples were formulated taking as reference previous studies.[40,47] A fixed quantity of the HDODA crosslinker (15 wt.%) and the TPO photoinitiator (7 wt.%) were mixed with the EGPEA, as monomer. Different amounts of PANI/MWCNT were added. Composite formulations are denoted by T7PCX where 7 indicates the amount of TPO and X is the PANI/MWCNT concentration by weight (Table 1).

The components were placed into vials and sonicated for 45 min using a Digital Sonifier at 10% of intensity (Branson 450) to promote homogeneous dispersion. Just before their use, samples were further mechanically stirred in a Vortex mixer for 2 min at 1000 rpm (VELP Scientific). The formulations were printed with a 3D printer (Elegoo mars PRO). The printer settings were adjusted based on the printer's technical requirements and the kinetics of polymerization of the formulations

tested. The light intensity of the 3D printer was 9 mW cm^{-2} and the exposure time per layer was adjusted for each formulation (Table 1). Bottom exposure, corresponding to the first 5 layers, was always subjected to a longer exposure time, to ensure that the sample adheres to the metal platform. The layer thickness (z) was set at 0.025 mm. It was noteworthy the printing difficulties of the T7PC3 formulation, due to its long curing times and adhesion problems to the printing platform. After multiple printing attempts, it was only possible to print three circles of 25 mm diameter to measure the electrical percolation threshold and thermal properties.

After printing, the samples were soaked in isopropanol for 10 min in order to remove the non-cured resin. A post-curing process was performed with a post-curing lamp (Form Cure, Formlabs) for 10 min at 35 °C. Flexible circular films of 25 mm diameter and dog-bone-shaped specimens according to ISO 527 were prepared to carry out the different tests.

Characterization of PANI/MWCNT Filler: The morphology of PANI/MWCNT powder and its individual constituents was evaluated by Transmission Electron Microscopy (TEM) (JEOL JEM 1010 (80 KeV), after applying 10 mL of the aqueous powder dispersions to a copper grid) and by Scanning Electron Microscopy (SEM) (JEOL JSM-7200F Field Emission Scanning Electron Microscope at an accelerating voltage of 10 kV).

The elemental analysis of C, H, N, and S was conducted in triplicate using ThermoFinnigan FlashEA1112 elemental analyzer (Conquer Scientific, Poway, CA, USA). The %PANI in the PANI/MWCNT composites was determined by Equation (1):

$$\exp \% PANI = \frac{\exp \% N \text{ in PANI/MWCNT}}{\exp \% N \text{ in pure PANI}} \cdot 100 \tag{1}$$

X-ray patterns were recorded in step-scan mode from 2° to 50° with a 2θ step of 0.05° using a D5000 diffractometer (XRD, Siemens-Bruker) with CuKα line irradiation (λ = 1.541 × 10–10 m). 40-point smoothing protocol using a Savitzky–Golay filter has been applied to the diffractograms (Origin 8.0 graphical software).

Raman spectroscopy analyses were carried out by Confocal Raman microspectroscopy, using a Thermo Scientific DXR3 spectrometer with a CCD camera, coupled to an Olympus confocal microscope. Raman spectra were acquired in the 3400–100 cm^{-1} region. The Raman scattering was excited using a diode laser at a wavelength of 532 nm. All spectra were collected by coadding 64 scans, with an acquisition time of 10 s. The laser beam was focused on the samples with a 10× microscope objective.

The Fourier Transformed Infrared (FTIR) spectra were recorded on a Jasco 4700 spectrometer equipment. Three absorption spectra were performed for each sample in Potassium Bromide (KBr) pellet with a 4 cm^{-1} resolution over 64 scans from 4000 to 400 cm^{-1} and the corresponding average spectra were examined.

The UV–vis spectra of 5 different suspensions (spanning from 30 to 200 ppm) of PANI and PANI/MWCNT in glycerin were recorded on a Jasco V-750 double-beam UV–vis spectrophotometer between 200 and 800 nm with a sampling interval of 1 nm and 25 accumulations.

Thermogravimetric Analyses (TGA) were performed using a TGA 4000–Perkin–Elmer set-up under nitrogen atmosphere supplied at a constant flow rate of 50 mL min^{-1}. The sample holders were ceramic crucibles with a capacity of 60 µL. The samples were subjected to a heating rate of 10.0 ± 0.1 °C min^{-1} in the temperature range between 50 to 700 °C.

Characterization of Acrylic 3D Printed Composites: The viscosity of the acrylic composites formulations was measured at room temperature using a controlled strain rheometer (ARES, TA Instruments) with parallel-plate geometry (25 mm diameter, 1 mm gap). The steady shear viscosity (η) was measured in a range of shear rates between 0.3 and 100 s^{-1}.

The kinetics of the UV-initiated radical polymerization of the acrylic composites with 0.5, 1,1.5, and 2 wt.% PANI/MWCNT were studied in situ by FTIR in the Attenuated Reflectance Mode (ATR) by using

2200590 (10 of 13)

**ADVANCED
SCIENCE NEWS**

www.advancedsciencenews.com

**ADVANCED
ELECTRONIC
MATERIALS**

www.advelectronicmat.de

an MK II Golden Gate Diamond 45° ATR accessory on the Jasco 4700 spectrometer. A droplet of each sample dispersion was applied on the center hole of a silicon wafer of 0.3 mm thick surrounding the ATR crystal of the FTIR spectrometer. Glass cover slips of 10×10 mm were placed on top of the liquid droplets after their application on the ATR crystal with the aim of controlling the thickness of the cured films and, simultaneously, reducing the diffusion of atmospheric oxygen into the resin.[48] The analyses were performed at least twice with a 4 cm^{-1} resolution between 1800 and 550 cm^{-1} over 5 scans (6 s). For each sample, a background measurement was run before its FTIR analysis. After collecting the first spectrum (time = 0) a Visicure 405 nm spot lamp, with an 8 mm diameter focus lens connected to a LED Spot-Curing System (BlueWave, Dymax Corp., Torrington, CT, USA), was turned on from the top side of the sample and repeated spectra were collected at 1 and 5 s intervals during 625 s to ensure high degrees of conversion, for the neat acrylic resin and the composites, respectively. The UV intensity was adjusted to reach a final intensity of 9 mW cm^{-2} over the sample, measured with a LED radiometer (Dymax ACCU-CAL 50-LED PN40519, Dymax Corp., Torrington, CT, USA). The spectra were subjected to baseline and ATR correction and analyzed using the Bruker OPUS software version 5.5 (Bruker Española S.A, Madrid, Spain). The degree of double bond conversion (DBC%) was calculated from the decrease in the area of the absorbance band located at 810 cm^{-1} (=CH stretching vibration of the acrylate group), normalized to the carbonyl ester stretching band ($\nu_{C=O}$) of the acrylic polymer at 1728 cm^{-1}, as internal reference, according to Equation (2):[48]

$$DBC\% = \frac{(A_{810}/A_{1728})_{t=0} - (A_{810}/A_{1728})_t}{(A_{810}/A_{1728})_{t=0}} \times 100\% \tag{2}$$

The subscript $t = 0$ indicates the peak areas of the liquid dispersion before UV irradiation, while the subscript t indicates the peak areas at time t of irradiation.

The conversion curves of DBC% versus time (s) were reasonably fitted with the Boltzman sigmoidal model.[74] Three regions can be distinguished in the graphs: the induction period after starting irradiation, the propagation region, and the equilibrium region or ultimate degree of conversion (DBC%). The maximum rate of polymerization (R_P) has been calculated by Equation (3) using the slope of the conversion versus time curves in the propagation region, for the conversion interval between 25–55%.

$$R_P = [M_0] \frac{(A_{810})_{t1} - (A_{810})_{t2}}{t_2 - t_1} \tag{3}$$

Where M_0 is the initial concentration of acrylate double bonds (which is 5.63 mol L^{-1} taking into account that HDODA is a bifunctional acrylate monomer and EGPEA is monofunctional), $(A_{810})_{t1}$ and $(A_{810})_{t2}$ are the areas of the band centered at 810 cm^{-1} at the irradiation times t_1 and t_2, corresponding to 25 and 55% conversion, respectively.

The morphology of the printed composites was evaluated by SEM. Specimens were broken under cryogenic conditions and examined using a JEOL JSM-7200F Field Emission Scanning Electron Microscope at an accelerating voltage of 10 kV. Prior to observation, the samples were sputter-coated with a thin palladium/platinum layer (Cressintong 208HR).

TGA of the acrylic films was performed as described in the previous section. Tensile stress–strain mechanical properties were characterized using an Instron 5569 universal testing machine (Instron Canton, MA) operating at room temperature and at a cross-head speed of 5 mm min^{-1} until failure. At least five dog-bone-shaped specimens were tested to evaluate the tensile properties according to ISO 527.

The room temperature electrical conductivity (σ) was calculated from the electrical resistance data by the four-probe method (LORESTA-GP, Mitsubishi Chemical, MCP-T610). The electrical conductivities (σ) reported for each sample are the mean values of at least 12 readings determined on three different samples. The minimum filler content that increases the electrical conductivity of the material in several orders of

magnitude, from insulating material to semiconductor or conductive material, was calculated on the basis of the electrical percolation threshold theory[74] according to Equation (4):

$$\sigma = \sigma_0(\rho - \rho_c)^t \tag{4}$$

where σ and σ_0 are the electrical conductivity of the composite and the effective conductivity of the PANI/MWCNT within the matrix, respectively; ρ is the concentration of the conductive filler inside the resin; t is a critical exponent that depends on the dimensions of the system, and ρ_c is the electric percolation threshold.[56]

Printable Composites for Force Sensor Devices: To elaborate the Jacobs working curves, the liquid formulations were cured over the screen of the printer 3D in circular films of 18 mm in diameter varying the exposure times. Every sample was performed in duplicate. After polymerization, the uncured material was clean up with 2-Propanol. The thicknesses of the samples were measured with a DUALSCOPE MP0R measuring instrument (Fisher) and plotted as a function of Exposure (E_{max}) (mJ cm^{-2}). According to Equation (5), the Jacobs working curve provided information about the penetration depth of the curing light and the energy required for polymerization.[75]

$$C_d = D_P \cdot \ln\left(\frac{E_{max}}{E_c}\right) \tag{5}$$

where C_d is the cured depth (µm), D_P is the penetration depth (µm) of the light source into the resin, E_{max} is the light irradiation dosage on the surface (mJ cm^{-2}), and E_c is the starting point for the transition from liquid to solid (mJ cm^{-2}).

Electromechanical tests were performed under cyclic compression on printed acrylic composites in a wide range of forces, 1, 3, 5, 10, 30, 50, 100, and 300 N, corresponding to 2, 6, 10, 19, 57, 96, 191, and 574 kPa, respectively, considering the contact area of the compression tests. The piezoresistive tests were performed in duplicate in a Shimadzu AG-IS universal testing machine with a load cell of 500 N at speeds between 0.5 to 5 mm min^{-1}, for 10 cycles. Force and displacement were recorded with a 500 ms time span. The acquisition of the electrical resistance of the compression pieces was performed with an Agilent 344401A multimeter. The electro-mechanical test results under compression were used to evaluate the pressure sensitivity (PS), according to Equation (6):

$$PS = \frac{\Delta R/R_0}{P} \tag{6}$$

where R_0 is the initial resistance in the unloaded state, ΔR represents the electrical resistance variation, and P is the applied pressure on the sample.

Supporting Information

Supporting Information is available from the Wiley Online Library or from the author.

Acknowledgements

Conflict of Interest

The authors declare no conflict of interest.

Author Contributions

G.A.-F.: Conceptualization, Methodology, Validation, Formal analysis, Investigation, Writing – Original Draft, Visualization. A.L.-L.: Methodology, Validation, Formal analysis, Writing – Original Draft, Visualization. A.A.-P.: Writing – Review & Editing. M.S.D.-G.: Conceptualization, Methodology, Validation, Writing – Review & Editing, Supervision. N.P.: Software. P.C.: Conceptualization, Methodology, Software, Writing – Original Draft, Visualization. S.L.-M.: Writing – Review & Editing, Supervision, Funding acquisition. M.-J.A.: Conceptualization, Writing – Review & Editing, Supervision, Project administration, Funding acquisition.

Data Availability Statement

The data that support the findings of this study are available from the corresponding author upon reasonable request.

Keywords

digital light processing, flexible electronics, multi-walled carbon nanotubes, piezoresistive pressure sensors, polyaniline, stereolithography

[1] C. Mendes-Felipe, J. C. Barbosa, S. Gonçalves, N. Pereira, C. M. Costa, J. L. Vilas-Vilela, S. Lanceros-Mendez, *Compos. Sci. Technol.* **2020**, *199*, 108363.

[2] R. Li, Q. Zhou, Y. Bi, S. Cao, X. Xia, A. Yang, S. Li, X. Xiao, *Sens. Actuators, A* **2021**, *321*, 112425.

[3] X. Wu, J. Wang, P. Li, X. Luo, Y. Yang, *IEEE Network* **2021**, *35*, 238.

[4] C. Mendes-Felipe, J. Oliveira, I. Etxebarria, J. L. Vilas-Vilela, S. Lanceros-Mendez, *Adv. Mater. Technol.* **2019**, *4*, 1800618.

[5] J. Huang, D. Li, M. Zhao, H. Ke, A. Mensah, P. Lv, X. Tian, Q. Wei, *Chem. Eng. J.* **2019**, *373*, 1357.

[6] Y. Song, H. Chen, Z. Su, X. Chen, L. Miao, J. Zhang, X. Cheng, H. Zhang, *Small* **2017**, *13*, 1702091.

[7] A. Reizabal, S. Gonçalves, R. Brito-Pereira, P. Costa, C. M. Costa, L. Pérez-Álvarez, J. L. Vilas-Vilela, S. Lanceros-Méndez, *Nanoscale Adv.* **2019**, *1*, 2284.

[8] S. Sharma, A. Chhetry, P. Maharjan, S. Zhang, K. Shrestha, M. Sharifuzzaman, T. Bhatta, Y. Shin, D. Kim, S. Lee, J. Y. Park, *Nano Energy* **2022**, *95*, 106970.

[9] G. Arias-ferreiro, A. Ares-pernas, A. Lasagabáster-latorre, M. S. Dopico-garcía, P. Ligero, N. Pereira, P. Costa, S. Lanceros-Mendez, M. Abad, *Adv. Mater. Technol.* **2022**, *2101503*.

[10] M. Amjadi, K. U. Kyung, I. Park, M. Sitti, *Adv. Funct. Mater.* **2016**, *26*, 1678.

[11] I. Cooperstein, E. Sachyani-Keneth, E. Shukrun-Farrell, T. Rosental, X. Wang, A. Kamyshny, S. Magdassi, *Adv. Mater. Interfaces* **2018**, *5*, 1800996.

[12] H. H. Hamzah, S. A. Shafiee, A. Abdalla, B. A. Patel, *Electrochem. Commun.* **2018**, *96*, 27.

[13] H. Jeong, Y. Cui, M. M. Tentzeris, S. Lim, *Addit. Manuf.* **2020**, *35*, 101405.

[14] D. A. Komissarenko, P. S. Sokolov, A. D. Evstigneeva, I. V. Slyusar, A. S. Nartov, P. A. Volkov, N. V. Lyskov, P. V. Evdokimov, V. I. Putlayev, A. E. Dosovitsky, *J. Eur. Ceram. Soc.* **2021**, *41*, 684.

[15] P. Costa, A. Ferreira, V. Sencadas, J. C. Viana, S. Lanceros-Méndez, *Sens. Actuators, A* **2013**, *201*, 458.

[16] L. Ma, X. Lei, S. Li, S. Guo, J. Yuan, X. Li, G. J. Cheng, F. Liu, *Sens. Actuators, A* **2021**, *332*, 113144.

[17] W. Zhao, Z. Wang, J. Zhang, X. Wang, Y. Xu, N. Ding, Z. Peng, *Adv. Mater. Technol.* **2021**, *6*, 2001218.

[18] J. Bhadra, N. J. Al-Thani, N. K. Madi, M. A. Al-Maadeed, *Arabian J. Chem.* **2017**, *10*, 664.

[19] H. Han, S. Cho, *Polymers* **2018**, *10*, 1003.

[20] H. Joo, S. Cho, *Polymers* **2020**, *12*, 67.

[21] E. N. Konyushenko, J. Stejskal, M. Trchová, J. Hradil, J. Kovářová, J. Prokeš, M. Cieslar, J.-Y. Hwang, K.-H. Chen, I. Sapurina, *Polymer* **2006**, *47*, 5715.

[22] F. S. Liu, J. X. Zheng, M. J. Huang, L. P. He, W. Q. Ao, F. Pan, J. Q. Li, *ACS Nano* **2010**, *4*, 2445.

[23] J. Zhang, A. Zhu, *Prog. Org. Coat.* **2021**, *159*, 106447.

[24] M. Rui, Y. Jiang, A. Zhu, *Chem. Eng. J.* **2020**, *385*, 123396.

[25] H. Zengin, W. Zhou, J. Jin, R. Czerw, D. W. Smith, L. Echegoyen, D. L. Carroll, S. H. Foulger, J. Ballato, *Adv. Mater.* **2002**, *14*, 1480.

[26] A. P. Francis, T. Devasena, *Toxicol. Ind. Health* **2018**, *34*, 200.

[27] L. Horta-Romarís, M.-J. Abad, M. V. González-Rodríguez, A. Lasagabáster, P. Costa, S. Lanceros-Méndez, *Mater. Des.* **2017**, *114*, 288.

[28] R. Jia, G. Shen, F. Qu, D. Chen, *Energy Storage Mater.* **2020**, *27*, 169.

[29] J. Stejskal, *Polym. Int.* **2019**.

[30] S. Jafarzadeh, P. M. Claesson, P. E. Sundell, E. Tyrode, J. Pan, *Prog. Org. Coat.* **2016**, *90*, 154.

[31] M. Sababi, J. Pan, P. E. Augustsson, P. E. Sundell, P. M. Claesson, *Corros. Sci.* **2014**, *84*, 189.

[32] A. B. Çiğil, E. A. Kandırmaz, H. Birtane, M. V. Kahraman, *Polym. Bull.* **2019**, *76*, 4355.

[33] G. Gonzalez, A. Chiappone, I. Roppolo, E. Fantino, V. Bertana, F. Perrucci, L. Scaltrito, F. Pirri, M. Sangermano, *Polymer* **2017**, *109*, 246.

[34] Q. Mu, L. Wang, C. K. Dunn, X. Kuang, F. Duan, Z. Zhang, H. J. Qi, T. Wang, *Addit. Manuf.* **2017**, *18*, 74.

[35] C. Mendes-Felipe, J. Oliveira, P. Costa, L. Ruiz-Rubio, A. Iregui, A. González, J. L. Vilas, S. Lanceros-Mendez, *Eur. Polym. J.* **2019**, *120*, 109226.

[36] L. A. Chavez, J. E. Regis, L. C. Delfin, C. A. Garcia Rosales, H. Kim, N. Love, Y. Liu, Y. Lin, *J. Appl. Polym. Sci.* **2019**, *136*, 47600.

[37] J. Huang, S. Virji, B. H. Weiller, R. B. Kaner, *Chem. - Eur. J.* **2004**, *10*, 1314.

[38] C. Oueiny, S. Berlioz, F. X. Perrin, *Prog. Polym. Sci.* **2014**, *39*, 707.

[39] A. Kolanowska, A. Wioleta Kuziel, R. Grzegorz Jedrysiak, M. Krzywiecki, E. Korczeniowski, M. Wísniewski, A. Piotr Terzyk, S. Boncel, *Nanomaterials* **2019**, *9*, 1619.

[40] G. Arias-Ferreiro, A. Ares-Pernas, M. S. Dopico-García, A. Lasagabáster-Latorre, M.-J. Abad, *Eur. Polym. J.* **2020**, *136*, 109887.

[41] O. Zhou, R. M. Fleming, D. W. Murphy, C. H. Chen, R. C. Haddon, A. P. Ramirez, S. H. Glarum, *Science* **1994**, *263*, 1744.

[42] J. P. Pouget, M. E. Józefowicz, A. J. Epstein, X. Tang, A. G. MacDiarmid, *Macromolecules* **1991**, *24*, 779.

**ADVANCED
SCIENCE NEWS**

www.advancedsciencenews.com

**ADVANCED
ELECTRONIC
MATERIALS**

www.advelectronicmat.de

[43] L. Liu, J. Yang, Y. Jiang, Y. Huang, Q. Meng, *Synth. Met.* **2013**, *170*, 57.

[44] T. Runka, *Phys. Sci. Rev.* **2017**, *2*, 20170025.

[45] D. Shao, G. Hou, J. Li, T. Wen, X. Ren, X. Wang, *Chem. Eng. J.* **2014**, *255*, 604.

[46] T. M. Wu, Y. W. Lin, *Polymer* **2006**, *47*, 3576.

[47] G. Arias-ferreiro, A. Ares-pernas, A. Lasagabáster-latorre, N. Aranburu, G. Guerrica-echevarria, M. S. Dopico-garcía, M. J. Abad, *Polymers* **2021**, *13*, 2068.

[48] S. Jafarzadeh, M. Johansson, P. E. Sundell, M. Claudino, J. Pan, P. M. Claesson, *Polym. Adv. Technol.* **2013**, *24*, 668.

[49] Z. Morávková, M. Trchová, E. Tomšík, J. Čechvala, J. Stejskal, *Polym. Degrad. Stab.* **2012**, *97*, 1405.

[50] Y. Yu, B. Che, Z. Si, L. Li, W. Chen, G. Xue, *Synth. Met.* **2005**, *150*, 271.

[51] B. Guo, X. Ji, W. Wang, X. Chen, P. Wang, L. Wang, J. Bai, *Composites, Part B* **2021**, *208*, 108598.

[52] A. Cortés, A. Cosola, M. Sangermano, M. Campo, S. González Prolongo, C. F. Pirri, A. Jiménez-Suárez, A. Chiappone, *Adv. Funct. Mater.* **2021**, *31*, 2106774.

[53] P. A. Kilmartin, *Chem. N. Z.* **2010**, 101.

[54] J. R. C. Dizon, A. H. Espera, Q. Chen, R. C. Advincula, *Addit. Manuf.* **2018**, *20*, 44.

[55] G. Scordo, V. Bertana, L. Scaltrito, S. Ferrero, M. Cocuzza, S. L. Marasso, S. Romano, R. Sesana, F. Catania, C. F. Pirri, *Mater. Today Commun.* **2019**, *19*, 12.

[56] P. Costa, J. Silva, V. Sencadas, R. Simoes, J. C. Viana, S. Lanceros-Méndez, *J. Mater. Sci.* **2013**, *48*, 1172.

[57] P. Wang, H. Chong, J. Zhang, H. Lu, *ACS Appl. Mater. Interfaces* **2017**, *9*, 22006.

[58] Y. Lin, S. Liu, L. Liu, *J. Mater. Chem. C* **2016**, *4*, 2353.

[59] E. Fantino, A. Chiappone, I. Roppolo, D. Manfredi, R. Bongiovanni, C. F. Pirri, F. Calignano, *Adv. Mater.* **2016**, *28*, 3712.

[60] C. Sciancalepore, F. Moroni, M. Messori, F. Bondioli, *Compos. Commun.* **2017**, *6*, 11.

[61] C. Qian, T. Xiao, Y. Chen, N. Wang, B. Li, Y. Gao, *Adv. Eng. Mater.* **2022**, *24*, 2101068.

[62] S. C. Tsai, L. H. Chen, C. P. Chu, W. C. Chao, Y. C. Liao, *Addit. Manuf.* **2022**, *51*, 102590.

[63] C. Mendes-Felipe, P. Costa, I. Roppolo, M. Sangermano, S. Lanceros-Mendez, *Macromol. Mater. Eng.* **2022**, *2100934*, 2100934.

[64] J. Vicente, P. Costa, S. Lanceros-Mendez, J. M. Abete, A. Iturrospe, *Materials* **2019**, *12*, 3545.

[65] J. T. Sutton, K. Rajan, D. P. Harper, S. C. Chmely, *ACS Appl. Mater. Interfaces* **2018**, *10*, 36456.

[66] J. Bennett, *Addit. Manuf.* **2017**, *18*, 203.

[67] F. P. W. Melchels, J. Feijen, D. W. Grijpma, *Biomaterials* **2010**, *31*, 6121.

[68] H. Gojzewski, Z. Guo, W. Grzelachowska, M. G. Ridwan, M. A. Hempenius, D. W. Grijpma, G. J. Vancso, *ACS Appl. Mater. Interfaces* **2020**, *12*, 8908.

[69] G. Ge, Y. Cai, Q. Dong, Y. Zhang, J. Shao, W. Huang, X. Dong, *Nanoscale* **2018**, *10*, 10033.

[70] Y. Wang, H. Mao, Y. Wang, P. Zhu, C. Liu, Y. Deng, *J. Mater. Chem. A* **2020**, *8*, 15167.

[71] N. Pereira, S. Gonçalves, J. C. Barbosa, R. Gonçalves, C. R. Tubio, J. L. Vilas-Vilela, C. M. Costa, S. Lanceros-Mendez, *Polymer* **2021**, *214*, 123349.

[72] J. Stejskal, R. G. Gilbert, *Pure Appl. Chem.* **2006**, *74*, 857.

[73] V. Tomeckova, F. Teyssandier, S. J. Norton, B. J. Love, J. W. Halloran, *J. Photochem. Photobiol., A* **2012**, *247*, 74.

[74] P. Costa, J. Oliveira, L. Horta-Romarís, M.-J. Abad, J. A. Moreira, I. Zapiráin, M. Aguado, S. Galván, S. Lanceros-Mendez, *Compos. Sci. Technol.* **2018**, *168*, 353.

[75] P. F. Jacobs, *Rapid Prototyping & Manufacturing. Fundamentals of StereoLithography*, 1st ed., Society of Manufacturing Engineers, United States of America **1992**.